URTeC: 1923519

Multiscale (nano to mm) Porosity in the Eagle Ford Shale: Changes as a Function of Maturity

L.M. Anovitz[1]*, D.R. Cole[2], A. Swift[3], J. Sheets[3], H. Elston[3], S. Welch[3], S.J. Chipera[4], K.C. Littrell[5], D.F.R. Mildner[6], M.J. Wasbrough[6]
1. Chemical Sciences Division, Oak Ridge National Laboratory; 2. School of Earth Sciences, Ohio State University; 3. School of Earth Sciences, Ohio State University; 4. Chesapeake Energy; 5. Chemistry and Engineering Materials Division, Oak Ridge National Laboratory; 6. National Institute of Standards and Technology, NIST Center for Neutron Research

Summary

Porosity and permeability are key variables that link the thermal-hydrologic, geomechanical and geochemical behavior in rock systems and are thus important input parameters for transport models. Recent neutron scattering studies have indicated that the scales of pore sizes in rocks extend over many orders of magnitude from nanometer pores with huge amounts of total surface area to large open fracture systems (multiscale porosity, cf. Anovitz et al., 2009, 2011, 2013a,b, Wang et al., 2013; Swift et al., in press). However, despite considerable effort combining conventional petrophysics, neutron scattering and electron microscopy, the quantitative nature of this porosity in tight gas shales, especially at smaller scales and over larger rock volumes, remains largely unknown (Clarkson, 2011). Nor is it well understood how porosity is affected by regional variation, thermal changes across the oil window and, most critically, hydraulic fracturing operations.

To begin providing this understanding we have used a combination of small and ultrasmall angle neutron scattering from the GP-SANS instrument at ORNL/HFIR, and the NG3-SANS (Glinka et al., 1998) and BT5-USANS instruments at NIST/NCNR (Barker et al., 2005), with SEM/BSE imaging to analyze the pore structure of clay and carbonate-rich samples of the Eagle Ford Shale. The Eagle Ford Shale is a late Cretaceous unit underlying much of southeast Texas and probably adjacent sections of Mexico. It outcrops in an arc from north of Austin, through San Antonio and then west towards Kinney County. It is hydrocarbon rich, straddles the oil window, and is one of the most actively drilled oil and gas targets in the US. The first successful horizontal well was drilled in 2008, and 2522 permits were recorded by Sept 1, 2011. While the oil and gas reserves in the Eagle Ford have been known since the 1970's, prior to the invention of horizontal drilling/hydraulic fracturing it was not considered economic.

Several important trends in the rock pore structure have been identified using our approach. Pore distributions are clearly fractal but, as was observed for the St. Peter sandstone (Anovitz et al., 2013a), are composed of several size distributions. Initial porosity is strongly anisotropic, as expected for shale. However, this decreases for shale, and disappears for carbonates with maturity. In both cases significant reduction occurs in total porosity, with most of the change coming at the finest scales (< ~ 10 nm), and an observable decrease at intermediate scales (near 100 nm)

Introduction

The US is at a turning point in the development of domestic resources, exploiting vast shale reserves for unconventional gas and oil. The USDOE notes that "Natural gas production from hydrocarbon rich shale formations, known as "shale gas" is one of the most rapidly expanding trends in onshore domestic oil and gas exploration and production today" (USDOE, 2009), and natural gas has been touted by some as a key "bridge fuel" that will transition the United States toward a lower-carbon energy economy. Estimates by the EIA of US reserves are very large (est. 1744 tcf), suggesting that they would supply the domestic US economy for 110 years, at a total annual production of volumes of 3 to 4 tcf, but this will depend on the efficiency of recovery. Even a small improvement in the recovery generated by an improved knowledge of the storage and release of the gas will have enormous benefit.

A number of interrelated properties control the amount of resources in the earth's crust that can be extracted from the target reservoir rock including temperature gradient, natural porosity and permeability, rock physical properties (e.g., elastic, brittle, thermal), the stress regime, total indigenous stored fluids and susceptibility to seismicity (e.g., Ingebritsen and Sanford, 1998; Ague, 2004; DOE-EGS, 2006). These factors, taken together, not only control the physical processes of extracting fluids, but also play a major role in determining the economics of energy production. While tight gas shales such as the Marcellus formation may contain enormous energy resources (Lee et al., 2011), the rate of gas flow through natural porosity is slow. Hence, hydraulic fracturing is necessary to recover the resource, and rocks with at least some connected permeability through fractures or pore spaces are more likely to result in a connected circulation system after stimulation. While fracture-dominated flow is highly relevant in shallow crustal settings, there is a continuum of coupled reaction/transport phenomena from the macroscale down to the finest nanopores that influence energy- and mass-transfer. Hydrocarbons, aqueous solutions, and volatile species (e.g., CH_4, CO_2,) can occupy and migrate through the pores or fractures of numerous types of complex heterogeneous earth materials present in the systems outlined above (Cole et al., 2004). Pores accessible to these fluids can span length scales (d as pore diameter or fracture aperture) ranging from < 1 nm to the cm scale and greater.

While the importance of porosity and pore-evolution has long been recognized (Johnson et al., 2004; Steefel et al., 2005), the contribution of nano- to microscale porosity to subsurface flow and retention has only recently been demonstrated (Kahle et al., 2004; Radlinski et al., 2004; Anovitz et al., 2009, 2011; Jin et al., 2011). In particular, limited attention has been paid to nanoporosity because the texture and overall volume of pores at the submicron scale have been difficult to characterize in a statistically meaningful manner. This is partly because of the diversity in pore morphology (i.e. length scales, pore shapes, connectivity, etc.) at this scale. While electron microscopy can provide detailed 2D images of pores at the nanoscale, the high magnification needed means that the total volume of the rock imaged is quite small, and therefore the results can be statistically questionable (Howard and Reed, 2005).

Nano- to micropores, because of their abundance and high surface to volume ratios, feature prominently in reactive transport modeling of many subsurface pore systems, particularly within low permeability lithologies. Pores in this size range include cracks, grain boundaries, fluid inclusions and single pores, and networks of pores of random shapes and orientations. While some nano- and micropores may be isolated from larger connected pores that control the bulk of the fluid flow volume, accessible, interconnected nano- and micropores may constrain overall flow at their pore throats and are the most likely sites for extensive fluid/rock reactions. In smaller pores, larger fractions of the pore fluid are in contact with the pore walls, possibly causing increased heat transfer from the rock to the fluid and, depending on the rock-fluid interactions, strong sorption effects (Rother et al., 2007). Indeed, nanopore confinement and pore wall interfacial interactions can alter fluid thermodynamics (Cole et al., 2009, 2010), and thus both the rates and equilibrium conditions of local reaction processes (Molins et al., 2012). In this context it is also extremely important to be able to characterize the nature of the pore wall chemistry through a detailed understanding of mineralogy as a function of pore size and type (Peters, 2009; Landrot et al., 2012). While flow at the outcrop and greater scale in many systems is likely to be controlled by macroscale pore and fracture systems, it may be the finer-

scale pore and fracture structures that control the access of fluids to the bulk of the rock, and thus much of the fluid-rock reactivity in the system (Shaw, 2005). Hence, it is vital to carefully define the reactive mineral surface area and pore connectivity at as many pore or fracture length scales as possible.

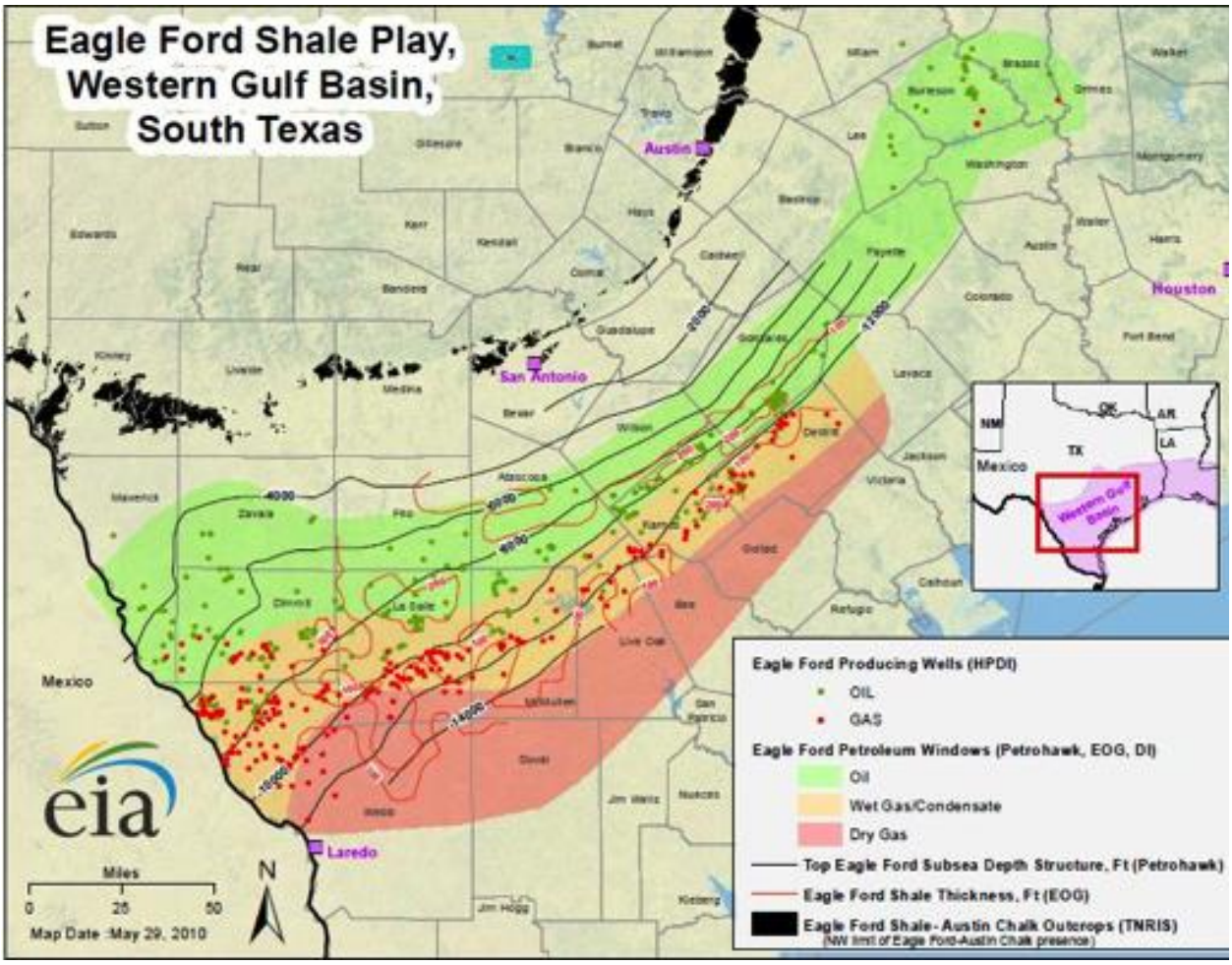

Figure 1: Map of the Eagle Ford shale (US Energy Information Administration and http://eaglefordshaleblog.com/2010/02/19/ eagleford-shale-maps/) Many additional wells have since been drilled, largely, but not exclusively, in the oil and wet gas regions.

Eagle Ford Shale

The Eagle Ford Shale is a late Cretaceous unit underlying much of southeast Texas and probably adjacent sections of Mexico. It outcrops in an arc from north of Austin, through San Antonio and then west towards Kinney County. It is hydrocarbon rich, and buried portions straddle the oil window (Fig. 1) The Eagle Ford is currently one of the most actively drilled oil and gas targets in the US. The first successful horizontal well was drilled in 2008, and 2522 permits were recorded (Texas Railroad Commission) by Sept 1, 2011. While the oil and gas reserves in the Eagle Ford have been known since the 1970's, prior to the invention of horizontal drilling/hydraulic fracturing it was not considered economic. As shown in Fig. 1, there are significant variations in pressure and depth across the field, which changes from oil-bearing to the northwest to gas in the southeast. The myriad of boreholes provide extensive sampling across the oil window.

Samples for this project were obtained from Chesapeake Energy. They consist of samples of clay-rich and carbonate rich lithologies from five drill cores obtained Frio, Zavala, Dimmit, LaSalle and Webb counties in southeast Texas. Depths range from 5512 to 8801 feet (from the surface), the sample cross the oil window from oil to gas-rich. Maturities were determined from controlled pyrolysis and measuring the peak evolution temperature - Tmax (e.g., RockEval or SRA), and ranged from $R_0 = 0.58$ to $R_0 = 1.57$.

Analysis of Porosity by Small Angle Neutron Scattering

The primary techniques used in this study to quantify porosity at scales below approximately 10 microns were small and ultrasmall-angle neutron scattering (U)SANS. (cf. Guinier and Fournet, 1955, Radlinski, 2006, Hammouda, 2009, Anovitz et al., 2009, 2011, 2013). Scattering contrast in rock samples arises primarily from the difference in the coherent scattering length densities (SLD) of the rock and the pores within it. The SLDs of different minerals in the rock are often similar, making mineral/mineral interface scattering contributions negligible. Thus, (U)SANS analysis provides a direct characterization of pore structure. Neutron beam cross sections are typically several cm^2, and cold neutrons are highly penetrating, compared with photons and electrons. Thus, the scattering curve results from a relatively large, and more statistically meaningful rock volume (typically ~ 30 mm^3, Anovitz et al., 2009). In addition, the high penetrating power of neutrons, relative to X-rays, allows analysis of thicker rock samples by neutron scattering. The SLD of phase j is given by:

$$r_j^* = \sum_{i=1}^{n} b_i \frac{r_j N_A}{M_i} \qquad (1),$$

where b_i is the bound coherent scattering length of atom i, N the total number of atoms in the molecule, ρ_j is the mass density, NA is the Avogadro constant and M_i is the molar mass. The total neutron scattering cross section for

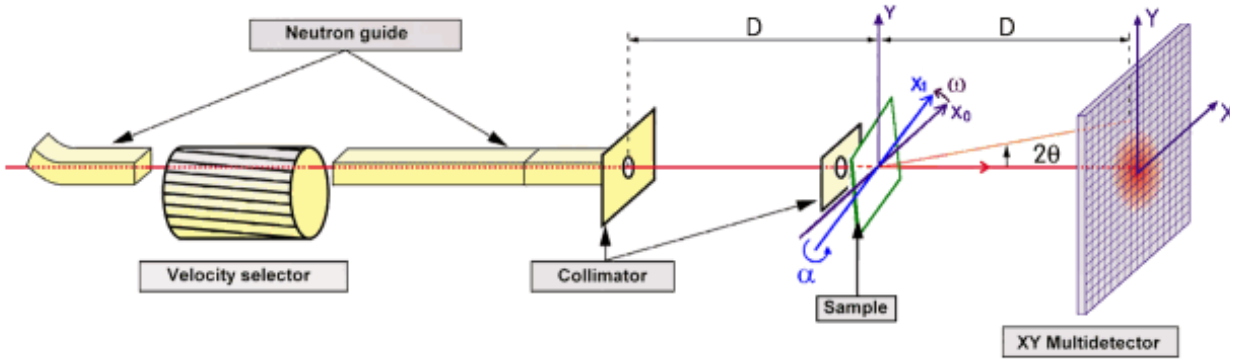

Figure 2: Schematic representation of a SANS experiment showing beam path, sample scattering and detector

hydrogen is large, allowing studies of water/rock interactions at nano- to micro-scales (and at various time scales with inelastic/ quasi-elastic scattering techniques). In fact, while the scattering cross section for X-rays is a function of the atomic number, that for neutrons is not, thus providing a significantly different, and very useful scattering contrast. Scattering from rocks occurs both from pores that are connected to the overall network and those that are not, and the large difference in SLD between hydrogen and deuterium means that the rock can be purposely saturated with a matrix contrast matched H_2O/D_2O mixture to separate connected from unconnected porosity, allowing a quantitative assessment of the interacting reservoir volume.

Figure 3: Detector tanks for two SANS instruments at the HFIR. The General Purpose SANS (with tank door open) and the bioSANS (nearer) are shown. The sample positions are at the other end of the tanks (far left).

A schematic of a pinhole SANS instrument is shown in. Fig. 2. After passing through a velocity selector neutrons propagate then down a long guide and through a collimation system. An aperture at the end of the collimator defines the cross section of the neutron beam interacting with the sample. The sample scatters a fraction of the neutrons, and the remainder are either transmitted or absorbed. The intensity of scattered and transmitted neutrons is measured with 1D or 2D detectors, normalized by the transmission and calibrated to absolute intensity.

The neutron detector resides in a large, cylindrical vacuum chamber (typically 10-20 m long) to reduce interference from air scattering (Fig. 3). The position of the detector and the beam stop can be varied to obtain a wider range of scattering angles. The Q ranges covered by SANS instruments vary somewhat, but are typically in the range from $1*10^{-3}$ $Å^{-1}$ < Q < 0.7 Å-1, which samples scattering features (e.g. pores) ranging from approximately 10 to 6000 Å.

Figure 4 shows a typical scattering pattern for a rock. This pattern is radially symmetrical if there is no preferred orientation in the sample, and is azimuthally averaged to obtain the scattering curve after appropriate corrections are applied. While the resultant integrated and normalized intensity could be plotted in terms of scattering angle, it is more commonly shown in terms of the momentum transfer vector Q (with units of $Å^{-1}$), defined as shown in Fig. 7, where Q is the momentum transfer, and E is the energy transfer. The USANS instrument uses a different design to measure scattering at lower Q. The USANS at NIST/NCNR covers a Q range from $4*10^{-5}$ $Å^{-1}$ < Q < $1*10^{-3}$ $Å^{-1}$, corresponding to measurement sizes in the range 100 nm to 20 μm (Barker et al., 2005, Hammouda, 2009). Thus, the two techniques are complementary. The USANS uses thermal neutrons (2.38 Å) and the Bonse-Hart method in

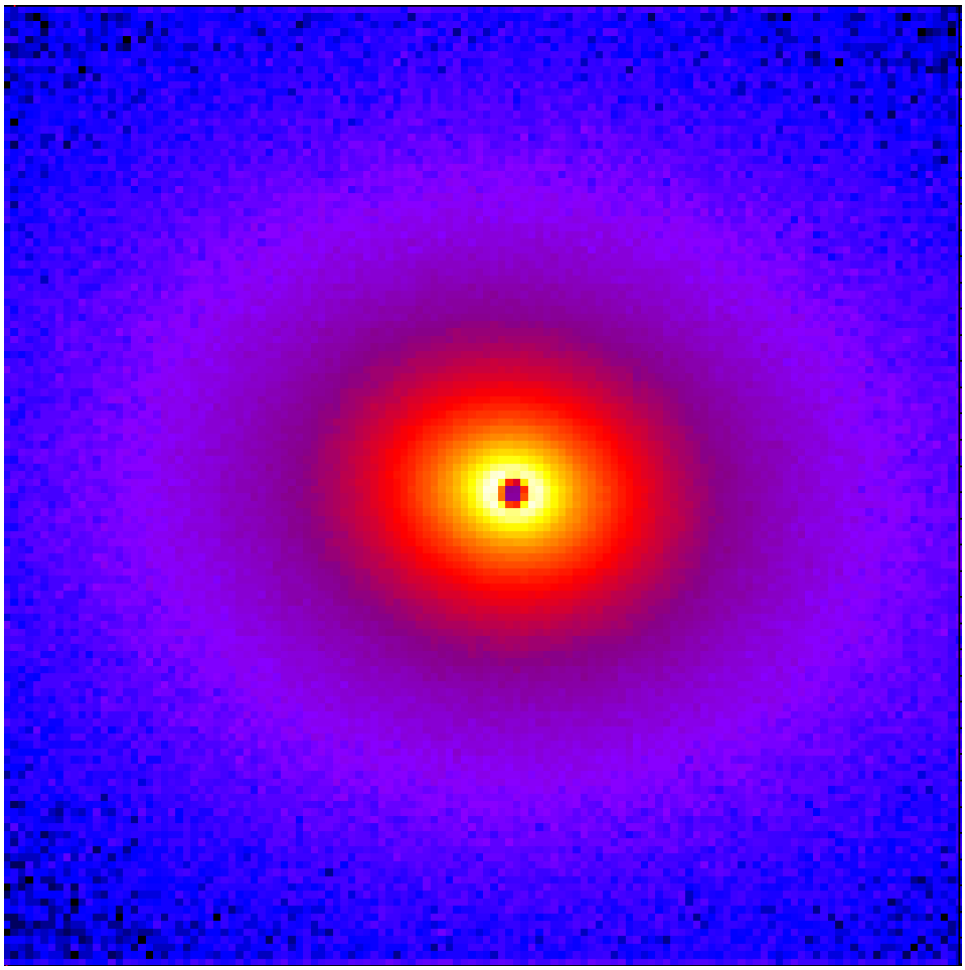

Figure 4: Example scattering data at a single detector distance for a sample of the Eagle Ford shale cut perpendicular to bedding. Intensities are higher near the direct beam (lower Q, larger scale lengths). Scattering is anisotropic for this sample, leading to apparent pore volume distributions that are directionally dependent.

which neutrons are monochromated by a triple-bounce, channel-cut single-crystal silicon monochromator, pass through the sample to another monochromator (as an analyzer) and finally to a detector. Scanning the analyzer yields the angular dependence of the scattering intensity. This allows a narrow wavelength resolution ($\Delta\lambda/\lambda$ = 0.059), but beam intensity is low relative to SANS, making count times longer. In addition, the use of a slit, rather than a pinhole geometry requires desmearing. Scattering data can be analyzed in reciprocal space by least-square fitting to model functions or in real space after Fourier transformation. Both techniques yield information about the shape and size or size ranges of scatterers. The invariant Z, defined by

$$Z = \int_0^{\infty} Q^2 I(Q) dQ \quad (2),$$

yielding direct, model-independent information about the scattering contrast and volume of scatterers. For a two-phase system the invariant is given by:

$$Z = 2p^2 f_1 (1 - f_1)(r_1^* - r_2^*)^2 \quad (3),$$

with φ_1 equal to the volume fraction of phase 1 and ρ_1* its coherent SLD. A great deal of other data can also be obtained from these scattering curves. Once the raw data have been reduced (cf. Kline, 2006), data yield the overall and cumulative porosities, pore distribution geometry (mass fractal behavior), the nature of the pore/rock interface (surface fractal behavior), characteristic lengths associated with the fractal behavior, and the surface area to volume ratio. Information on the pore size distribution and connectivity provides key insight into capillary pressure behavior and liquid storage in the reservoir.

In many cases, even the combination of SANS and USANS does not cover a sufficiently large Q range to describe the complete scattering curve for many rocks. There are several approaches to filling this gap, including backscattered electron (SEM/BSE) imaging (Radlinski et al., 2004, Anovitz et al., 2013a). We have developed an autocorrelation approach based on this kind of imaging and have coupled it with X-ray CT imagery as part of this study (see below). While neutrons are very penetrating, suitable sample thickness is important. If the sample is too thin, scattering power will be low. If too thick, multiple scattering lowers scattering intensity at low Q and raises it at higher Q, distorting the signal. Anovitz et al. (2009) showed that, for limestone samples, a thickness of 150 microns was suitable. We typically prepare samples by mounting them on quartz glass plates 1mm thick (Anovitz et al., 2009). If such samples are not available, however, well cuttings cast into epoxy blocks and then sectioned may be used, although this limits the availability of information on porosity at the largest (cm) scales. Neutron scattering has the advantage over high magnification electron and X-ray imaging techniques of providing statistically meaningful characterizations averaged over large volumes of material.

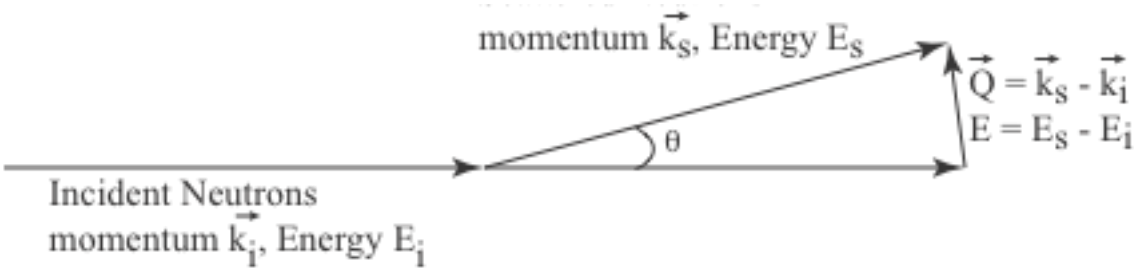

Figure 5: Vector diagram showing the origin of the Q vector.

While electron microscopy can provide detailed images of pores at high magnifications, the total volume of the rock imaged is, of necessity, very small. At lower magnifications, however, imaging techniques can be used to extend the range of scattering data from ~ 10 microns to ~ 1 cm using backscattered electron imaging with SEM, or X ray computed tomography following the work of Debye et al. (1957), Radlinski et al. (2004) and Anovitz et al. (2013a). This approach calculates the autocorrelation curve from such images, the Fourier transform of which provides a further extension of the scattering curve. Together, these techniques provide quantitative characterization of rock porosity at scales ranging from ~ 1 nm to greater than 1 cm – roughly 7 orders of magnitude.

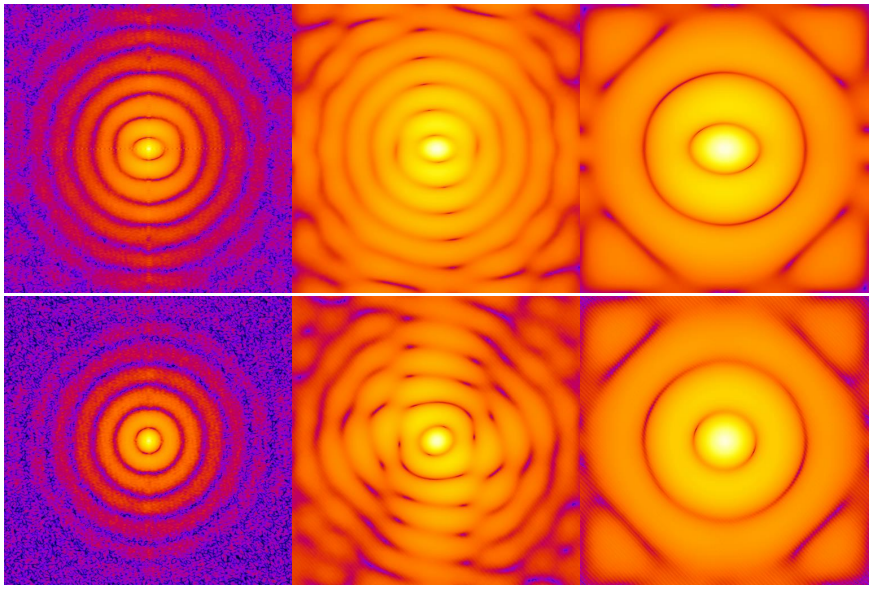

Figure 6: Autocorrelation analysis of the lowest (top) and highest (bottom) maturity carbonate-rich samples. The three images for each were calculated from scattering patterns obtained at detector distances of 1, 4 and 13 meters (left to right) on NG3-SANS instrument at NIST/NCNR. Focusing on the innermost ring, note the change in symmetry with increasing maturity.

The Effects of Maturation on Multiscale Porosity in the Eagle Ford Shale

At the current time, two caveats must be considered when interpreting (U)SANS data for shales. The first is the two-phase assumption. Radlinski (2006) noted that, because the scattering length densities of most minerals are reasonably similar, and because scattering contrast varies as the square of the difference in the scattering length densities, scattering from rocks can be treated as if there are only two "phases" present – rock with a scattering length density equal to the volume-weighted average of the phases present (often near the value for quartz, 4.08 x 10^{-6} Å^{-2}), and pores. However, this is not quite as true for shales in which the scattering length densities of the minerals range from a high of approximately 5.4 x 10^{-6} Å^{-2} for dolomite, to a low of approximately 3.17 x 10^{-6} Å^{-2} for illite, complicated by the quite variable, and often unknown values for the organic matter itself. Thus, while scattering from mineral/mineral interfaces is still significantly weaker than that from mineral/pore interfaces, it may still be significant, especially if the number of mineral/mineral interfaces is large, as is likely the case for fine-grained rocks such as shales. For the purposes of this paper, however, an average scattering length density comprised of the weighted average of the mineral phases, and considering the organic matter as scattering like empty pores will be used. For this reason the calculated porosity will be referred to as "apparent porosity."

The second caveat concerns the interpretation of the scattering anisotropy. As shown in Figure 4, the scattering patterns obtained from low maturity samples cut perpendicular to bedding are highly anisotropic. Analysis of sections cut parallel to bedding, however, yields isotropic scattering patterns. Thus, the three dimensional scattering pattern is an ellipsoid of rotation, and all of the potential information can be obtained from the single sample cut perpendicularly. However, while apparent porosities can be calculated parallel to, and perpendicular to the bedding, pore volumes are inherently three dimensional, and the anisotropy must disappear if the sample is homogenized. This implies that the apparent directional differences are due to projection of what is clearly a-three dimensional anisotropy onto a two-dimensional plane. This suggests two possibilities. Either, the total porosity in each direction

will be equivalent, if differently distributed, if all Q–values could be measured, or a correction factor for the effect of the projection is needed. For the purposes of this paper, however, a limited-Q range analysis of directionally dependent apparent porosity will be used.

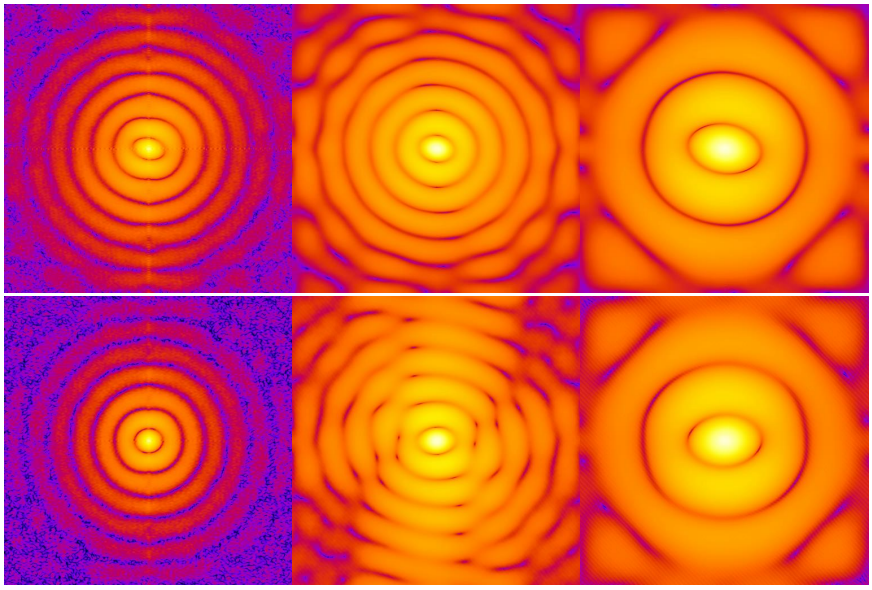

Figure 7: Autocorrelation analysis of the lowest (top) and highest (bottom) R_0 clay-rich samples. The three images for each were calculated from scattering patterns obtained at detector distances of 1, 4 and 13 meters on NG3-SANS instrument at NIST/NCNR. As with the carbonate-rich samples increasing maturity reduces the asymmetry. In the case, however, this is incomplete at the largest scales.

One useful way to qualitatively examine changes in the structure of apparent porosity is to examine two-dimensional autocorrelation figures calculated from the two dimensional scattering patterns. This converts the inverse-space scattering data to real-space. Results for the highest, and lowest-R_0 carbonate rich samples are shown in Fig. 6, and those for the clay rich samples in Fig. 7. Three figures are presented for each as data were collected on the NG3 SANS instrument at NIST/NCNR at three different detector distances, 1, 4 and 13 meters (left to right on the plot), equivalent to size ranges of approximately 16 Å to 6300 Å. The symmetry, or lack thereof, for each pattern is most clearly represented in the innermost ring. It is clear from Figs. 6 and 7 that maturation dramatically reduces the asymmetry of the submicron structure of the shale, but that the extent of this effect is composition-dependent. In the carbonates the asymmetry is essentially completely destroyed at all scales. In the clay-rich shales, however, while the asymmetry at the finer scales is eliminated, that at the larger scales is not. Similar results were observed in experimental studies of the effects of heating on shale microstructures (Littrell et al., 2011).

The apparent porosity is also greatly reduced in the (U)SANS range (that is, for pores with a radius below about 8 microns) during maturation. The lowest maturity carbonate-rich sample has an apparent porosity of 42.6 % parallel to bedding, and 17.0 % perpendicular to bedding, and the lowest maturity clay-rich sample has an apparent porosity of 40.9 % parallel to bedding, and 12.8 % perpendicular to bedding. By contrast, however, the highest maturity carbonate-rich sample has an apparent porosity of 3.5 % parallel to bedding, and 3.1 % perpendicular to bedding, and the lowest maturity clay-rich sample has an apparent porosity of 21.1 % parallel to bedding, and 11.4 % perpendicular to bedding. Again, it is clear from these data that the anisotropy is essentially eliminated in the

carbonate-rich sample, but only reduced, along with the overall porosity, in the clay-rich sample, although these values are, of course, subject to the assumptions described above.

Interestingly, these results are in direct contradiction to some results observable at larger scales. Figure 8 shows to backscattered electron images of organic-filled pores in the low and high-R0 clay-rich samples. It is clear from these images that porosity has dramatically increased inside the organic material during maturation. However, because the scattering length density of the organics themselves are relatively low (if specifically unknown), and thus more similar to that of unfilled pores that the surrounding mineral grains, it is likely that scattering from these pore structures is relatively weak. The scattering observed, therefore, is largely due to intergranular porosity, as well as contributions from mineral/mineral interfaces.

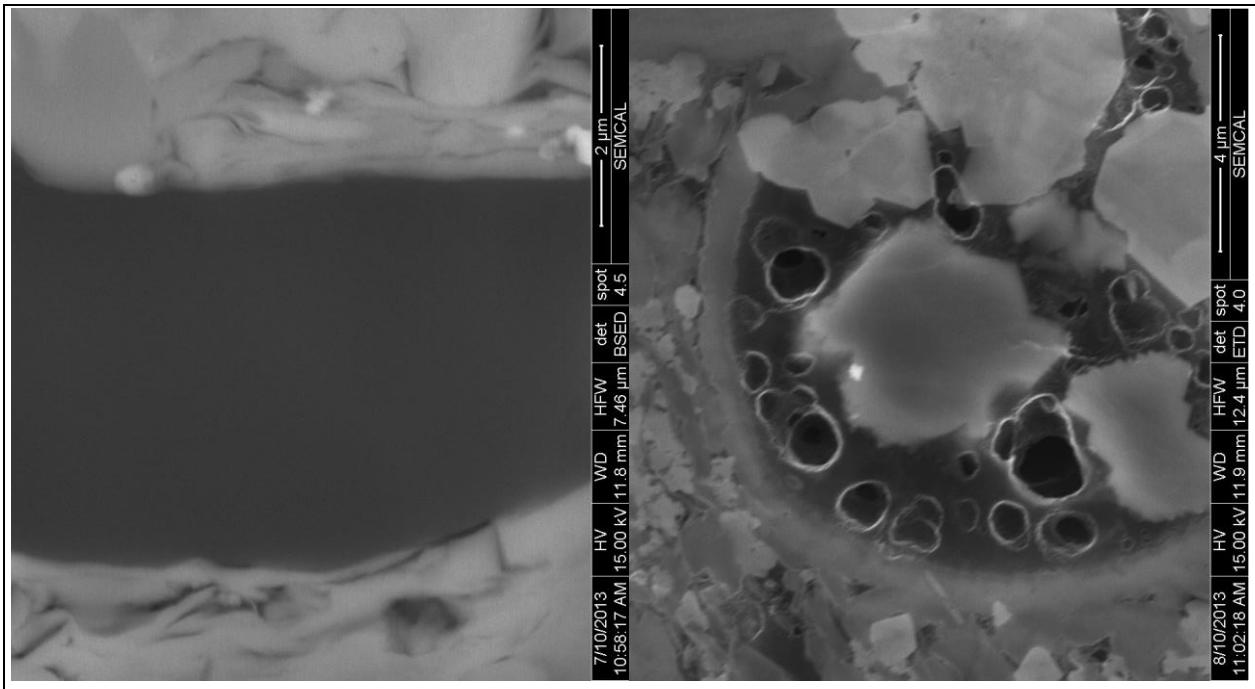

Figure 8: Backscattered electron images taken on a FEI field emission secondary electron microscope of the clay-rich samples. The dark areas are organic-filled pores. The low R_0 sample on the left shows no evidence of porosity in the organic material, while pores have clearly formed, probably due to gas formation, in the high R_0 sample at the right.

Conclusions

The data presented here clearly show that small angle scattering techniques can be of significant importance in understanding the evolution of porosity in the rocks hosting unconventional oil and gas resources over a wide range of scales. Neutron scattering results show a decrease in overall apparent porosity, as well as pore structure asymmetry at scales from approximately 1 nm to 10 µm, but imaging suggests that porosity within the organic deposits increases over this same range. These effects are, however, variable as a function of the mineralogy of the sample (clay- vs. carbonate-rich).

The variability in pore features and associated mineralogy we observe will have a profound impact on the fracture properties of the formation and development of flow permeability as a consequence of hydraulic fracturing, as well as changing the fracture characteristics of the rock. Thus the best strategies for oil and gas recovery are likely to vary

across the Eagle Ford and other tight gas shales are likely to vary with maturity, and multiscale pore assessment can thus be a vital component is assessing best practices used when developing a strategy for efficient oil and gas recovery.

Acknowledgements

Effort by LMA, was supported by research sponsored by the Division of Chemical Sciences, Geosciences, and Biosciences, Office of Basic Energy Sciences, U.S. Department of Energy. DRC, AS, JS, SW and HE were funded by the Department of Energy Office of Basic Energy Sciences, Division of Chemical Sciences, Geosciences and Biosciences through the Energy Frontier Research Center - Nanoscale Control of Geologic CO_2. The samples analyzed were kindly provided by Chesapeake Energy. We acknowledge the support of the National Institute of Standards and Technology, Center for Neutron Research, U.S. Department of Commerce, and the High-Flux Isotope Reactor at the Oak Ridge National Laboratory in providing the research neutron facilities used in this work. This work utilized facilities supported in part by the National Science Foundation under agreement No. DMR-0944772. Certain commercial equipment, instruments, materials and software are identified in this paper to foster understanding. Such identification does not imply recommendation or endorsement by the National Institute of Standards and Technology, the Department of Energy, or the Oak Ridge National Laboratory, nor does it imply that the materials or equipment identified are necessarily the best available for the purpose.

References

Ague, J. J. (2004) Fluid flow in the deep crust. In. Treatise of Geochemistry, Vol. 3 The Crust, R. L. Ridnick (ed.), 195-228.

Anovitz, L.M., Lynn, G.W., Cole. D.R., Rother, R., Allard, L.F., Hamilton, W.A., Porcar, L., and Kim, M.-H. (2009) A new approach to quantification of metamorphism using ultra-small and small angle neutron scattering. Geochimica et Cosmochimica Acta, 73, 7303-7324.

Anovitz, LM, Rother, G, and Cole, DR. (2011) Characterization of rock pore features in geothermal systems using small angle neutron scattering (SANS). Proc. 36th Workshop On Geothermal Res. Eng., Sgp-Tr-191, 571-582.

Anovitz, LM, Cole, DR, Rother, G, Allard, LF JR., Jackson, A, and Littrell, KC (2013a) Diagenetic changes in macro-to nano-scale porosity in the St. Peter Sandstone: an (Ultra) small angle neutron scattering and backscattered electron imaging analysis. Geochimica et Cosmochimica Acta, 102, 280-305.

Anovitz, LM, Wang, H-W, Cole, DR, Sheets, J, Rother, G, Faulder, DD, Walters M (2013b) Analysis of Multiscale Porosity at the Coso Geothermal Field. Proc. 38th Workshop On Geothermal Res. Eng., SPG-TR-198.

Barker, J.G., Glinka, C.J., Moyer, J.J., Kim, M.H., Drews, A.R. and Agamalian, M. (2005) Design and performance of a thermal-neutron double-crystal diffractometer for USANS at NIST. J. Appl. Crystallogr. 38, 1004–1011.

Clarkson, C.R. (2011) Reservoir engineering for unconventional gas reservoirs: what do we have to consider. SPE 145080, 45 p.

Cole, D. R., Gruszkiewicz, M. S., Simonson, J. M., Chialvo, A. A., Melnichenko, Y. B., Wignall, G. D., Lynn, G. W., Lin, J. S., Habenschuss, A., Gu, B., More, K. L., and Burchell, T. D. (2004) Influence of nanoscale porosity on fluid behavior, Water-Rock Interaction, vol. 1, no. Editors: R. Wanty and R. Seal, p. 735-738.

Cole, D. R., E. Mamontov, and G. Rother (2009) Chapter 19. Structure and dynamics of fluids in microporous and mesoporous earth and engineered materials, in Liang, L., R. Rinaldi, and H. Schober, eds., Neutron Applications in Earth, Energy, and Environmental Sciences, Springer, p. 547-570.

Cole, D. R., A. A. Chialvo, G. Rother, L. Vlcek, and P. T. Cummings, 2010, Supercritical fluid behavior at nanoscale interfaces: Implications for CO_2 sequestration in geologic formations, Philosophical Magazine, Special Issue on Layer Silicate materials and Clays, vol. 90, no. 17-18, p. 2339-2363.

Debye P, Anderson, Jr., HR and Brumberger H (1957) Scattering by an inhomogeneous solid. II. The correlation function and its application. J. Appl. Phys. 28, 679–683.

DOE-EGS (2006) The Future of Geothermal Energy: Impact of Enhanced Geothermal Systems (EGS) on the United States in the 21st Century. http://www1.eere.energy.gov/geothermal/egs_technology.html

Glinka, C. J., Barker, J. G., Hammouda, B., Krueger, S., Moyer, J., and Orts, W. (1998) The 30m SANS instruments at NIST. J. Appl. Cryst. 31, 430-445.

Guinier, A and Fournet, G (1955). Small Angle Scattering of X-rays. New York: John Wiley.

Hammouda, B (2009) Probing Nanoscale Structures. The SANS Toolbox, book available online at http://www.ncnr.nist.gov/staff/hammouda/the_sans_toolbox.pdf

Howard, C.V. and Reed, M.G. (2005) Unbiased Stereology (Garland Science/BIOS Scientific, New York).

Ingebritsen, S. E. and Sanford, W. E. (1998) Groundwater in Geologic Processes. Cambridge University Press, 341 pg.

Jin, L., G., Rother, Cole, D. R., Mildner, D. F. R., Duffy, C. J., and Brantley, S. L. (2011) Characterization of deep weathering and nanoporosity development in shale - a neutron study, American Mineralogist, vol. 96, p. 498-512.

Johnson, J. W., Nitao, J. J., and Knauss, K. G. (2004) Reactive transport modeling of CO_2 storage in saline aquifers to elucidate fundamental processes, trapping mechanisms and sequestration partitioning. In: *Geological Storage of Carbon Dioxide* (S. J. Barnes and R. H. Worden, eds.) Geological Society, London Spec. Pub. 233, 107-128.

Kahle, A., Winkler, B., Radulescu, A. and Schreuer, J. (2004) Small angle neutron scattering study of volcanic rocks, European Journal of Mineralogy, vol. 16, p. 407-10.

Kline SR (2006) Reduction and analysis of SANS and USANS data using IGOR Pro. J. Appl. Crystallogr. 39, 895–900.

Landrot, G., Ajo-Franklin, J., Yang, L., Cabrini, S., and Steefel, C. I. (2012) Measurement of accessible reactive surface area in a sandstone, with implications to CO2 mineralization, Chemical Geology, vol. 318-319, p. 113-125.

Littrell, KC, Rother, G., Anovitz, LM, Debeer-Schmitt, CLM (2011) In-situ study of kerogen release and metamorphism in oil shale by SANS. 7th International Symposium on Novel Materials and their Synthesis. IUPAC, Shanghai, China, Oct, 2011.

Molins, S., Trebotich, D., Steefel, C. I. and Shen, C. (2012) An investigation of the effect of pore scale flow on average geochemical reaction rates using direct numerical simulation, Water Resources Research, vol. 48, no. 3, W03527.

Peters, C. A. (2009) Accessibilities of reactive minerals in consolidated sedimentary rock: an imaging study of three sandstones, Chemical Geology, vol. 265, p. 198-208.

Radlinski, AP, Ioannidis, MA, Hinde, AL, Hainbuchner, M, Baron, M, Rauch, H, and Kline, SR (2004) Angstrom-to-millimeter characterization of sedimentary rock microstructure. J. Colloid Interface Sci 274, 607-612.

Radlinski, AP (2006) Small-angle neutron scattering and rock microstructure. In: Neutron Scattering in Earth Sciences, ed. by H-R Wenk, Reviews in Mineralogy and Geochemistry 63, 363-397.

Rother, G., Melnichenko, Y. B., Cole, D. R., Frielinghaus, H. and Wignall, G. D. (2007) Microstructural characterization of adsorption and depletion regimes of supercritical fluids in nanopores, Journal of Physical Chemistry C, vol. 111, p. 15736-15742.

Shaw, R. P. (2005) Understanding the Micro to Macro Behavior of Rock–Fluid Systems (No. 249), London, Geological Society of London, 176 p.

Swift, A, Anovitz, LM, Sheets, JM, Cole, DR, Welch, SA, Rother, G (in press) Relationship between Mineralogy and Porosity in Caprocks Relevant to Geologic CO2 Sequestration. Environmental Geosciences.

Steefel, C. I., DePaolo, D. J. and Lichtner, P. (2005) Reactive transport modeling: An essential tool and a new research approach for the Earth science, Earth and Planetary Science Letters, vol. 240, p. 539-558.

UDSOE (2009) Modern shale gas development in the United States: a primer. April, 2009.

Wang, H-W, Anovitz, LM. Burg, A, Cole, DJ, Allard, LF, Jackson, AJ, Stack, AG, and Rother, G (2013) Multi-scale characterization of pore evolution in a combustion metamorphic complex, Hatrurium basin, Israel: Combining (ultra) small-angle neutron scattering and image analysis. Geochimica et Cosmochimica Acta, 121, 339-362.